FINAL PUBLISHABLE REPORT

Grant Agreement number	17FUN04
Project short name	SEQUOIA
Project full title	Single-electron quantum optics for quantum-enhanced measurements

Project start date and duration:	01 May 2018, 42 months	
Coordinator: Dr Frank Hohls, PTB Tel: +49 531 5922530 E-mail: frank.hohls@ptb.de Project website address: https://www.ptb.de/empir2018/sequoia/project/		
Internal Funded Partners: 1. PTB, Germany 2. LNE, France 3. NPL United Kingdom	External Funded Partners: 4. CEA, France 5. CNRS France 6. LatU Latvia	Unfunded Partners
RMG –		

TABLE OF CONTENTS

1 Overview

This project developed new measurement techniques to support the development of semiconductor quantum technology. These techniques were based on the use of quantum techniques, namely on-demand single-electron quantum optics, where the quantum properties of moving electrons within a semiconductor device are examined and used. The new metrological tools developed by the project have enabled the characterisation of (i) the quantum state of electrons in semiconductor quantum devices and (ii) quantum enhanced sensing based on the technique of single-electron quantum optics. The project's approach used the control, transfer, manipulation and measurement of on-demand single-electron wave packets. The project has also developed a solid-state on-demand single-electron interferometer for the time-resolved direct on chip measurement of local fields, as used to manipulate e.g. quantum states in electronic quantum devices. Furthermore, the project developed tools for the characterisation of the on-demand single-electron quantum state.

2 Need

The first quantum revolution resulted in ground-breaking technologies such as the transistor and the laser. A second quantum revolution is expected to bring transformative advances to key areas of science, industry and technology. Consequently, the European Commission launched a quantum technology flagship in 2018 to foster the role of European industry and research in this area.

New quantum technologies will allow the exploitation of quantum effects for enhanced sensing or for the metrology of single particles; however, such new technologies will also need new measurement capabilities. For applications like quantum computation and simulation, scalable quantum technology needs to be developed. Semiconductor quantum devices have demonstrated the potential for complex integrated quantum circuitry. However, a prerequisite for using the electron quantum state as a resource is the ability to characterise its properties. In addition, the control of quantum states needs exact knowledge of local magnetic and electric fields, via in-situ time-resolved sensing.

These needs for the metrology of electron quantum states and for in-situ fast quantum sensors were addressed by harnessing the properties of on-demand electron wave packets. By analogy with the use of photons in quantum optics, the transmission and manipulation of on-demand electron wave packets has allowed the realisation of 'electron quantum optics' which can be used for sensitive quantum-enhanced measurements.

To support these important technological developments in semiconductor quantum technology, the project has also produced a metrology toolbox for (i) the sourcing and detection (Objective 1), (ii) testing and validation (Objective 2), and (iii) quantum state tomography (Objective 4) of single-electron wave packets. Furthermore, on-chip quantum sensing was developed using single-electron wave packet interferometry (Objective 3). Therefore, this project has delivered the much needed, metrological foundation for future scalable solid-state quantum device applications and has enabled the development of semiconductor-based quantum information technology.

3 Objectives

The goal of this project was to develop new measurement techniques to support the development of semiconductor quantum technology. These techniques were based on the use of a new field of quantum techniques, namely on-demand single-electron quantum optics, where the quantum properties of moving electrons within a semiconductor device are examined and used. The specific objectives for the project were:

1. **To produce semiconductor device components for on-demand single-electron quantum optics-based sensing and state tomography**, including quantum dot based high-energy on-demand synchronised single-electron sources for time-resolved interferometry, single-charge detectors for electron quantum optics, and correlation measurement techniques and devices for quantum state metrology.
2. **To develop the metrological tools for the verification of single-electron sources required for the assessment and optimisation of the emitted electron wave packet states**, including the characterisation of the dynamic electron state within the source quantum dot and the indistinguishability test of the travelling single-electron wave packet.

3. **To develop an experimental technique for on-demand single-electron wave packet interferometry for the sensing of local magnetic and electric fields with high time resolution** (~ 1 ns or below) and high spatial resolution (~ 1 µm).
4. **To develop concepts and theoretical tools for full quantum state tomography to enable the realisation of quantum enhanced measurements using electron wave packets.**
5. To foster the application of single-electron wave packet devices for quantum metrology and the European metrology capabilities for quantum technology.

4 Results

4.1 Semiconductor device components for on-demand single-electron quantum optics-based sensing and state tomography (Objective 1)

Objective 1 for the project was to produce semiconductor device components for on-demand single-electron quantum optics-based sensing and state tomography, including quantum dot based high-energy on-demand synchronised single-electron sources for time-resolved interferometry, single-charge detectors for electron quantum optics, and correlation measurement techniques and devices for quantum state metrology. The goals of this objective were

- to provide the necessary technology for semiconductor device components, in order to fabricate devices for different metrological applications based on single-electron wave packets and
- to provide the necessary experimental techniques for the implementation of the single-electron quantum optics experiments.

4.1.1 Basic building blocks for single-electron quantum optics

Quantum dot based high-energy sources of single-electrons: These sources generate single-electron wave packets and inject these into the quantum Hall edge channels, which guide the wave packets through the circuit. For interferometry experiments, energy and time matching of electron emission from multiple sources is important. The error rate of the pumps with a typical target value of better than 10^{-3} should not restrict the overall fidelity of the circuit. The exit barrier of each pump can easily be used to fine-tune the emitted energy over a range of meV, however larger adjustment typically disturbs the number of electrons loaded/ejected per cycle, requiring retuning of other controls.

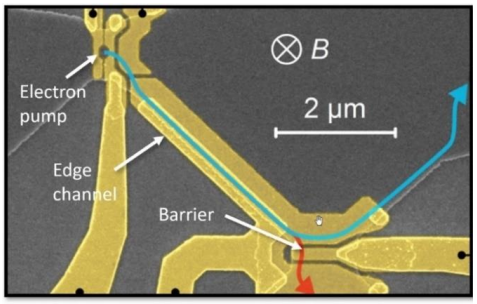

Figure 1: Example device with single pump, wave guide and analyser/filter barrier

To improve energy alignment, in particular for multiple pumps, PTB used an additional tuning gate, which controlled the barrier symmetry of the pump and allowed the shifting of the emission profile of the pump over a wide range of energies. After several device iterations and adjustments to the gate geometries of the quantum dot sources, the requirements of the circuit applications were successfully met and subsequently devices of this type were fabricated and examined by NPL and PTB.

Quantum point contacts and beam splitters: Energy selective transmission barriers provide the ability to probe and filter the incident electron beam dependent on the distribution of emission time and energy. The resolution of tomographic back-projection protocols and measurements of the arrival time distribution benefit from a highly selective barrier, whereas the visibility in interferometers requires an energetically flat transmission profile with respect to the width of the emission distribution. Results from the time of flight and tomography experiments were then used by NPL and PTB to improve the device layout.

Transmission lines: Transmission lines (of various dimensions) are a basic element of any circuit configuration and were used by PTB and NPL to characterise ballistic transport, i.e., different energy relaxation mechanisms and time of flight. Test structures were routinely produced to validate low loss single-electron transmission in quantum hall edge channels and to provide quantification of the transverse confinement energy. The results of the characterisation of ballistic transport measurements were then used to improve the tunability of confinement energy and reduce losses due to scattering by partners NPL and PTB.

4.1.2 Shot noise correlation measurement setups

Noise measurements in single-electron systems can be (i) a readout of particle number, (ii) used to probe indistinguishability, and (iii) used to perform single-electron tomography. Measurement of the partition noise in single-electron devices, when combined with simultaneous measurements of the average current, gives access to the statistics of the electron scattering process for single or multiple electrons arriving at a barrier.

The electrons from a pump transmitted at barrier with probability T give current $I_T = Tef$; I_T is therefore some fraction of ef ~ 100 pA and can be recovered with a current-to-voltage converter.

The noise component is more difficult to measure as the size of the current spectral density $S_I = 2T(1-T)e^2f$ is much smaller than other sources typically found in the system (e.g. amplifier and Johnson noise in the sensing resistor). However, systems have been developed that use low noise cryogenic amplifiers and sampling on multiple channels/ohmic contacts.

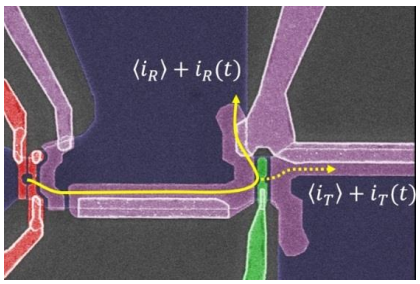

Figure 2: Single-electron partitioning at a barrier: Time-varying and average current contains complementary information about scattering statistics

Work was performed by CEA and NPL on probes of the indistinguishability of single-electron wave-packets. CEA and NPL have each developed respectively. improved measurement systems based on dry ^{3}He/^{4}He dilution refrigerators which have the following key features:

- CEA - Two channel setup, digital sampling and cross correlation, resonance circuits with centre frequencies 1.8/2.5 MHz,
- NPL - 1 minute type A uncertainty of 0.8/1.3·10^{-30} A^2/Hz.

4.1.3 Devices for trapping and detecting high energy single-electron wave packets

PTB has detected the outcome of each experimental cycle with a charge detector in order to analyse the outcome of single-electron quantum optics circuits. Injected electrons were trapped at the circuit's output and then detected. The basic detection scheme required four components: (i) a single-electron source, (ii) a ballistic waveguide, (iii) a detection node (see above for details on these components), and (iv) a charge detector dot.

Single-charge detectors: The trapping and detection scheme for ballistic electrons requires two components. Firstly, ballistic electrons are trapped by controlled energy relaxation on a detection node and secondly the charge state of the node is read out by a detector quantum dot. The combination of these two components have been successfully used by PTB to achieve a sufficiently high enough level of sensitivity to resolve single-electrons reliably (charge state separation > 10 σ) and maintain stability for the accumulation of a large enough statistical basis (> 10^6 events) to accurately evaluate the full counting statistics.

The complexity of a integrated single-electron quantum optics circuit with all the above components means that it requires a high-quality material platform and highly reliable and reproducible lithography. In terms of material quality PTB used devices with a geometry similar to Figure 1 to identify suitable PTB-grown wafer materials with low impurity-induced scattering and negligible random telegraph noise. PTB tested a variety of wafers from in total three sources (including two samples provided by NPL for comparison). Wafers grown with highly purified Gallium (Ga) stood out as the best and were selected for use in circuits.

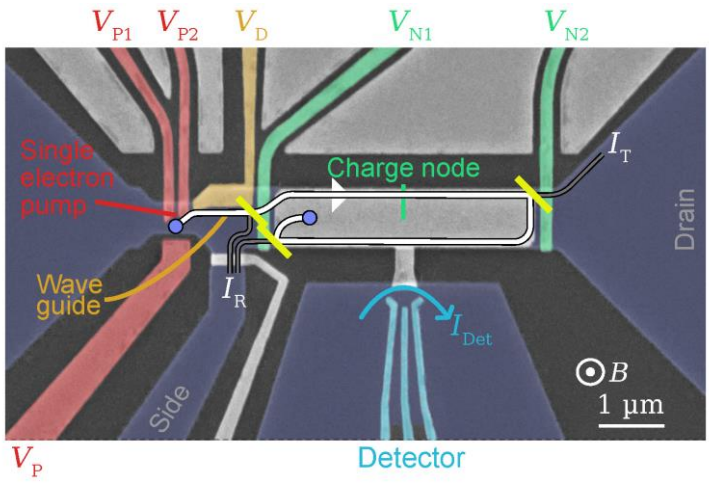

Figure 3 False colour SEM image of a sample implementing all components necessary to demonstrate the ballistic transport and trapping of high-energy electrons. Etched mesa conductive region (dark blue), gates forming the single-electron pump (red), edge depletion gate (orange), node confining gates (green) and detector dot gates (cyan) are coloured. White lines indicate the path of an electron being trapped inside the node, grey lines sketch multiple paths of electrons ending up in one of the leads. The device and further similar devices are used in section 4.2.2.

A comparison with model calculations for the emission of longitudinal-optical phonons showed good agreement with the predictions of the emission rate in a parabolic transverse confinement. It also provided an in-situ measurement method for characterising the device-dependent transverse confinement energy without the need for a dedicated test structure. PTB also improved the lithography quality to a very high level (e.g. geometry variation < 10 nm), which resulted in reliable fabrication of working circuits.

Figure 3 shows the circuit used to demonstrate trapping and detection of single-electron wave packets as a metrological tool (see Objective 2 and Section 4.2.2 for more details). The circuit was established as both as characterisation tool (on its own) and as a component for even more complex circuits e.g. Hong-Ou-Mandel (HOM) setups.

Multiple charge detectors could be operated simultaneously when integrated into a HOM circuit configuration and could be used to measure coincidence correlations. An example measurement result of a two-detector correlation measurement for emission of multiple electrons from one source is presented in Objective 2 and Section 4.2.2.

4.1.4 Devices for graphene breakdown assessment

To characterise Quantum Hall Effect (QHE) breakdown properties in hexagonal-boron nitride (h-BN) encapsulated graphene, two devices with a Hall bar geometry (width of 4 µm) were fabricated at CEA from heterostructures made of a graphene monolayer encapsulated between h-BN flakes of a few tens of nanometres thickness (see Figure 4a).

A graphite back-gate was added to tune the carrier density and to screen charged impurities located in the Silicon dioxide/Silicon (SiO_2/Si) substrate on which the stack was deposited. The stack was made using polypropylene carbonate (PPC) transfer of mechanically exfoliated layers obtained from high-purity crystals. The device mesa was defined by Trifluoromethane/Oxygen (CHF_3/O_2) reactive ion etching and Chromium/Gold (Cr/Au) contacts which were realised at the stack edges.

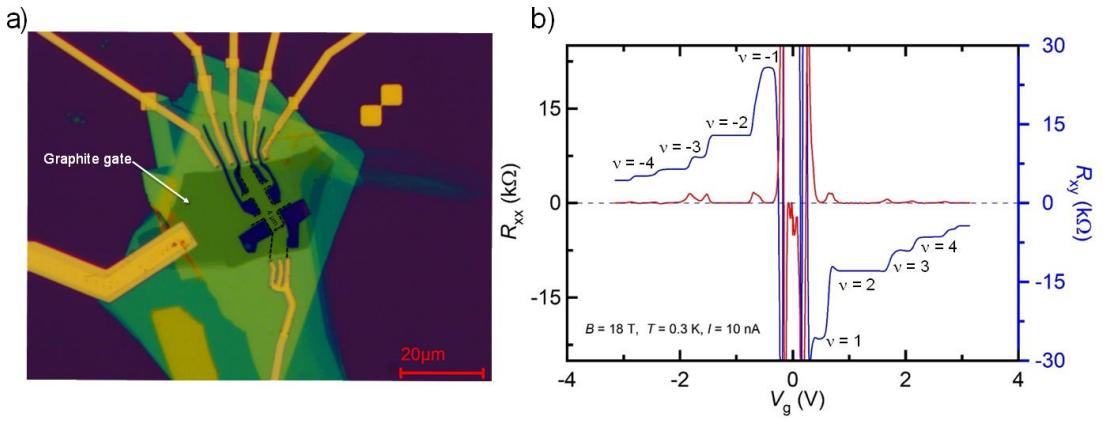

Figure 4 a) Optical image of a h-BN encapsulated graphene Hall bar. b) Magnetoresistance measured at B=18 T. This and further devices of similar type are used in section 4.2.1

The resistance of contacts was measured in the QHE regime ($\nu = 2$ plateau) using a three-terminal connection scheme in order to use the edge equipotentiality.

In the first Hall bar (S1), contact resistances of approx 100 Ω were typically measured, which corresponded to a contact resistivity of approx 350 Ω μm. To further improve the quality of these contacts, which are known to be critical not only for achieving an accurate quantised Hall resistance but also for observing the fractional QHE, a more complex design was tested for the second Hall bar (S2). In the S2 device, the graphite gate surface was reduced so that the carrier density of an area close to the contacts could be independently tuned and increased by the Si back-gate. This achieved a lower contact resistivity of approx 250 Ω μm.

From magnetoresistance measurements performed at low magnetic fields, an unexpectedly low carrier mobility of approx 2000 $cm^2V^{-1}s^{-1}$ was determined for carrier densities of a few 10^{11} cm^{-2} in the S1 device. This unexpectedly low carrier mobility was explained by pollution or water that got in between the layers during stack manufacturing.

Carrier mobilities close to 100000 $cm^2V^{-1}s^{-1}$ and 70000 $cm^2V^{-1}s^{-1}$ at 4 K for holes and electrons respectively were measured in the S2 device. These higher carrier mobilities allowed the observation of the QHE below 1 T and an increase of both spin and valley degeneracies of Landau levels at 18 T (see Figure 4b)). In addition, typical features of the fractional ± 4/3 state were observed at B =19 T and T = 0.3 K.

The S1 and S2 devices of different mobilities were subsequently used to explore dissipation mechanisms in the QHE regime, see Objective 2 and Section 4.2.1.

4.1.5 HOM type devices and experimental setups

Two-particle interference effects can reveal information about the quantum indistinguishability of single- electron wave packets. A conceptually simple method of performing these measurements is to directly collide two electrons from different sources at a beam splitter and then consider the scattering outcomes within the expectations of quantum exchange statistics. This method is akin to the HOM optical configuration which enables the observations of the indistinguishability and size of photon wave packets.

In the beam splitter method, the experimental signature of indistinguishability driven by exchange statistics is an excess 'antibunching' i.e. electrons leave the beam splitter in different output channels, in contrast to a random process. In fact, any interaction that perturbs the electronic state of each input electron can affect the partitioning process, thus coulomb interactions may also be present. There are many demanding and technical aspects when using the beam splitter method to study electronic interactions at the single particle level. As part of the project, partners NPL, PTB and CNRS have performed extensive work on device design, fabrication, testing, tuning, measurement, and analysis to enable measurements of single-electron interaction (as described in the subsections below).

Using devices fabricated in GaAs, NPL and PTB used continuously operated single particle sources of the tuneable barrier type to inject electrons into high energy chiral edge channels. Conditioning of the path between

the source and the interaction region was managed with gated edges (see Figure 5 and Figure 6). The HOM experiment itself was performed using different approaches.

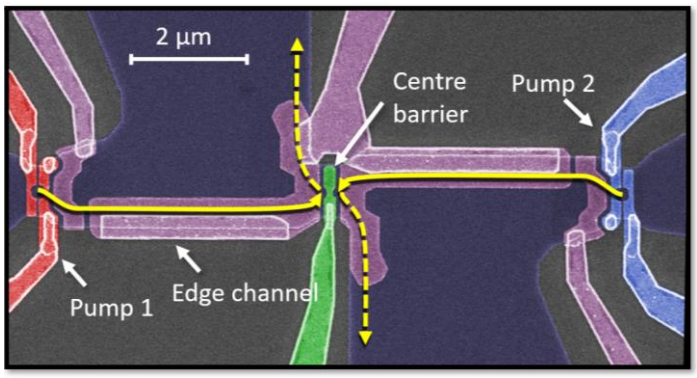

Figure 5: Example HOM device with two pumps and central barrier

HOM experiments with DC current and noise readout at NPL: Energy matching was performed using previously established spectroscopic techniques. Synchronisation was performed by applying a short synchronisation pulse to the central partitioning barrier and then studying the partitioned current. Distribution of the partitioned current was measured with shot noise amplifiers. From the combination of mean current and fluctuations NPL was able to deduce the partition statistics of the two-electron partitioning at the barrier.

HOM with Single shot readout (PTB): To use the accuracy provided by on-demand electron sources, a combination of a trapping node and a capacitively coupled quantum dot for charge readout were added by PTB to the circuit. The entrance barrier to the trapping node acted as an energy filter to capture electrons which had traversed the circuit without energy loss (Figure 6). Using the counting scheme also detailed in Section 4.1.3 (device) and Section 4.2.2 (mechanism and demonstration) coincidence correlations between the two charge detector signals were measured in a single shot mode. The full counting statistics that could be acquired in this setup provided accurate access to every possible outcome of the collision experiment. One electron source provided the reference electron with fixed energy/time distribution and emission energy and the injection time of the second electron were varied to test indistinguishability.

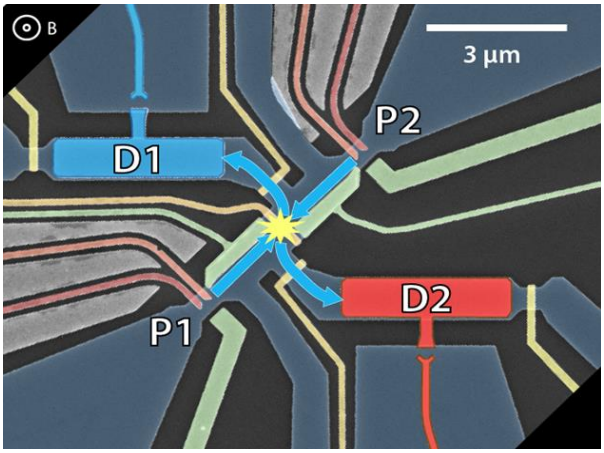

Figure 6: A HOM-circuit configuration to measure coincidence correlations using single shot read out. In addition to the elements seen in Figure 5, two charge detector circuits (D1, D2) were used to capture the electrons after the collision at the central barrier.

HOM devices for low-energy single-electrons (CNRS): Devices with a HOM arrangement for low-energy sources (e.g. Levitons) were fabricated at CNRS using techniques already established for previous studies of two particle interference.

4.1.6 Manufactured devices for single-electron interferometry

Two different types of interferometers were investigated: (i) Mach-Zehnder interferometers at CEA, PTB and NPL, and (ii) Fabry-Perot interferometers at CNRS.

Fabry-Perot interferometers have the advantage of a simpler geometry and a simpler fabrication process. However, multiple paths can occur within the cavity are allowed, which means that different phase shifts for different round trips inside the cavity, need to be taken into account, hence this makes the analysis more complex. In addition, the possibility of trapping electrons inside the cavity leads to stronger effects on the Coulomb interaction, which again makes the analysis more complex and tends to suppress the dependence of the interference pattern on the magnetic flux.

In contrast, Mach-Zehnder interferometers define only two paths for interferometry, leading to a simpler analysis. In addition, effects of the Coulomb interaction are smaller which allows complete modulation of the interference pattern with the magnetic flux, which is a better configuration for magnetic field sensing. However, in the original design of a Mach-Zehnder interferometer, an ohmic contact in the centre of the interferometer is needed to absorb the current in the first interferometer output, which leads to fabrication issues when wanting to shrink the size of interferometer.

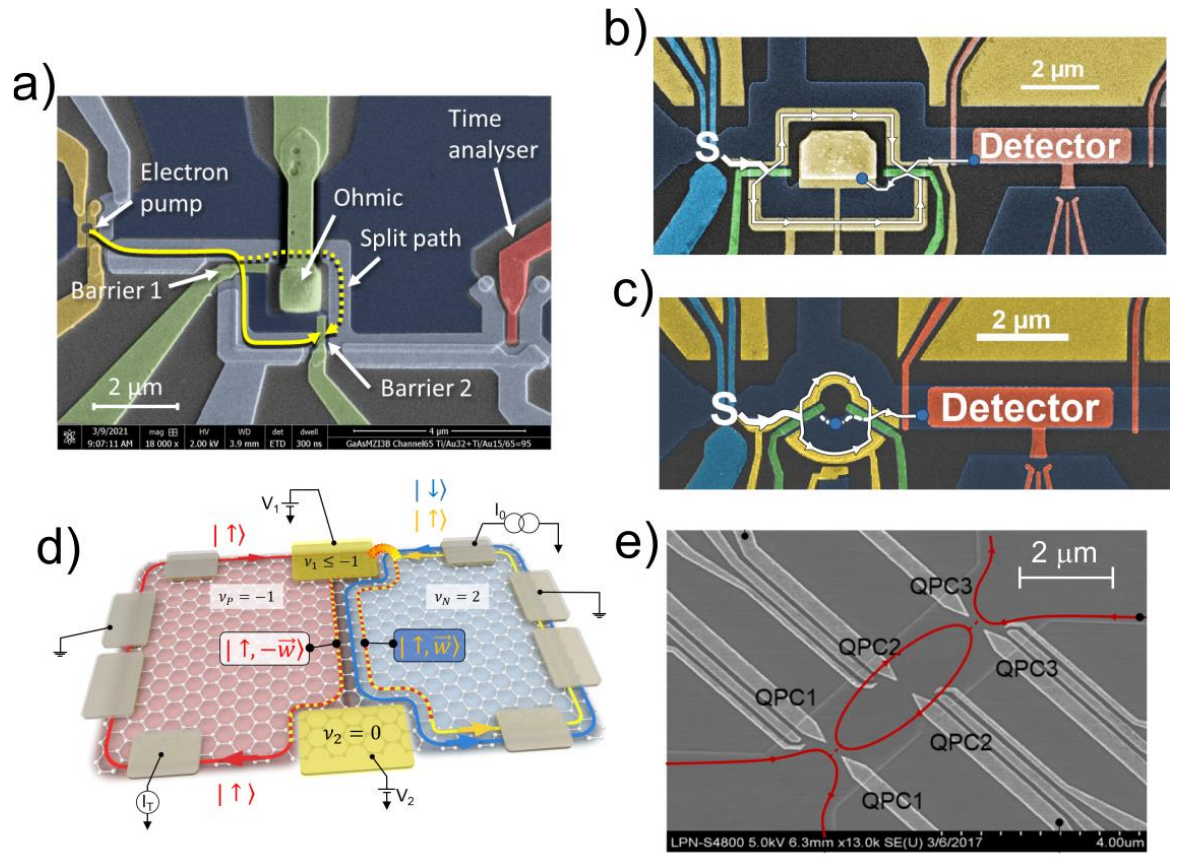

Figure 7: SEM pictures of the interferometers realised. a) Mach-Zehnder interferometer fabricated in GaAs at NPL. An electron pump at the input of the interferometer generated hot electrons. The characteristic size of the interferometer is 2 microns. b) First design of Mach-Zehnder interferometers in GaAs fabricated at PTB. Hot electrons are emitted by a fast pump and can be detected at the output by a single-electron detector. The characteristic size of the interferometer is 4 microns. c) Second design of interferometers at PTB which eliminates the central ohmic contact reducing the interferometer's size to below 2 microns. d) Sketch of the Mach-Zehnder interferometer fabricated in graphene by CEA. The two beam-splitters are located at the interface of a p-n junction between a v=2 and a v=-1 region. e) Fabry-Perot interferometer in GaAs fabricated at CNRS. Two quantum point contact are used as beam-splitters, defining the input and outputs of the Fabry-Perot cavity. The characteristic cavity size of 4 microns. Single-electron wave-packets are generated by applying Lorentzian voltage pulses at the input of the interferometer.

Additionally, two types of single-electron sources were investigated. (i) Hot electrons (emitted at a typical energy of 10-100 meV) and generated by fast single-electron pumps were studied at PTB and NPL. (ii) CNRS and CEA investigated low energy electrons generated by applying voltage pulses of Lorentzian shape with a typical energy of a few tens of µeV above the Fermi energy.

Each of the 2 sources i.e. hot electrons and low energy electrons had its own merits. Hot electrons are less sensitive to thermal fluctuations and can be emitted with very short temporal width (typically 10 ps) for optimum temporal resolution. Energy relaxation can also be mitigated which has not been demonstrated with low energy electrons. However, the coherence time of hot electrons has not been measured yet, therefore the factors limiting the contrast of interferometers in single-electron interferometry are unknown yet. In contrast, electronic

interferences have already been observed with low-energy electrons, but their temporal width is larger (few tens of picoseconds) which leads to a lower time resolution.

Finally, two types of materials were investigated, Gallium Arsenide (GaAs) and graphene. GaAs benefits from the availability of significant previous experience on the design of small electronic interferometers. Recently Mach-Zehnder interferometers have also been realised in graphene and have shown very compact geometries with excellent visibilities (for details of the realisation using a p-n-junction [9].

4.1.7 Conclusions

Objective 1 to produce semiconductor device components for on-demand single-electron quantum optics-based sensing and state tomography, including quantum dot based high-energy on-demand synchronised single-electron sources for time-resolved interferometry, single-charge detectors for electron quantum optics, and correlation measurement techniques and devices for quantum state metrology was fully achieved by the project.

The project developed successfully performed a theoretical study, that offers guidance for the optimisation of energy relaxation in hot electron quantum optics via acoustic and optical phonon emission. The project also performed experimental studies to examine, the energy relaxation as a function of emission energy for different energy ranges, path geometries, electrode designs and settings. In addition, a comparative study was performed on the electron relaxation mechanisms due to electron-electron interactions and optical phonon emission in GaAs semi-conductor systems using a variety of wafer materials. In the comparative study the scattering rates were found to be strongly dependent on the wafer material. For high energy electron wave packets survival probabilities larger than 97 % were demonstrated for a path length of several microns, which was sufficiently large for integration into more complex semiconductor devices.

Further to this, the project demonstrated single-electron wave packet capture and detection with a fidelity of 99.9 %, thus providing a new route for the realisation of single-electron quantum optics.

Finally, the project has successfully demonstrated the use of a quantum Hall valley beam splitter in a p-n junction in graphene which is an important step towards the tomography of single Leviton excitations in graphene. The beam splitter transmission could be tuned from zero to near unity and was controlled by tuning the mixing point of edge channels at the corner of a p-n junction by an electrostatic side gate.

4.2 Metrological tools for the verification of single-electron sources required for the assessment and optimisation of electron wave packet states (Objective 2)

Objective 2 for the project was to develop the metrological tools for the verification of single-electron sources required for the assessment and optimisation of the emitted electron wave packet states, including the characterisation of the dynamic electron state within the source quantum dot and the indistinguishability test of the travelling single-electron wave packet. The goal of this objective was to provide new techniques for the characterisation and detection of electron wave packet states. For certain applications this wave packet metrology can then also be used to optimise the single-electron state with respect to the applications requirements. Different aspects and technologies were examined.

The first of the subsections below summarises the exploration of dissipation and breakdown in the QHE regime in h-BN encapsulated graphene as basis for developing this new, explorative platform for single- electron/hole quantum optics. The subsequent subsections then describe the results from the GaAs/ Aluminium Gallium Arsenide (AlGaAs) technology platform: firstly, the development of techniques for capture and detection of individual single-electron wave-packets which were applied as new tool for metrology with and of electron wave packets. Then secondly, the development of new tomography techniques for single- electron wave-packets.

4.2.1 Dissipation in the QHE regime in h-BN encapsulated graphene

The development of a single-electron interferometry platform based on graphene requires high-quality devices operating in the QHE regime. In particularly the dissipation mechanisms responsible for electron backscattering need to be determined. These investigations are also essential for testing the Hall quantisation accuracy of graphene-based quantum resistance standards which require a low rate of charge carrier backscattering [5].

Considering this information, one important question for this project was whether a higher carrier mobility, than that achieved in graphene grown on Silicon carbide (SiC) (typically 10000 $cm^2V^{-1}s^{-1}$), will lead to a resistance standard operating in more relaxed experimental conditions, i.e. at lower magnetic field (B < 3.5 T), higher temperature (T > 10 K) or higher measurement current (I > 500 µA)?

Another important question for this project was whether the sharp increase of the longitudinal voltage, which results in the breakdown of the QHE beyond a threshold current value, could be used as a very sensitive current detector, possibly able to detect the injection of a Leviton quasi-particle.

The following results were gained by LNE (measurement and analysis) with the support of CEA for device fabrication, (see Objective 1 and Section 4.1.4). The quantisation of the Hall resistance in the QHE regime relies on the absence of backscattering: i.e. the two-dimensional gas must be in a dissipation-less state. At a finite temperature and measurement current, a residual level of dissipation exists and can be quantified by the measurement of the longitudinal resistance. The analysis of the dependency of current and temperature on the longitudinal conductivity allowed LNE to determine the mechanisms of dissipation, i.e., of backscattering.

Temperature dependence - The measured conductivity can be explained by the backscattering mechanism based on the variable range hopping (VRH), both in the low carrier mobility (device S1) and the high carrier mobility device (S2, both from Objective 1, Section 4.1.4). The temperature data can be fitted by the law of the VRH based on a soft Coulomb gap

$$\propto \left(\frac{1}{T}\right) \exp\left[-(T_0/T)^{-1/2}\right]$$

where $T_0 = C\frac{e^2}{4\pi\epsilon_0\epsilon_r\xi}$, ξ is the localisation length and $C = 6.2$ is a numerical parameter related to percolation theory.

In device S1 the maximal value of T_0 amounted to approx 1850 K at $B = 16\,T$. A similar value was found in a device of the same carrier mobility but made of graphene grown by chemical vapor deposition (CVD) of propane/hydrogen on SiC. In contrast, in the high carrier mobility device (S2) T_0 was approx 40000 K at $B =$ 10 T. This reflects stronger temperature robustness of the dissipation-less state.

For comparison, the highest values were found at approx 10000 K in devices made of graphene grown on SiC. In these devices, the localisation length deduced from such a large T_0 value is lower than the magnetic length $l_B = \sqrt{\hbar/eB}$, which is not expected from the VRH theory. This disagreement seems to occur in a highly robust dissipation-less state independently of the nature of the graphene material.

Current dependence – In the VRH theory based on a soft Coulomb gap, the longitudinal conductivity follows

$$\propto \exp\left[-(I_0/I)^{-1/2}\right]$$

where I_0 is is linked to T_0 by $T_0 = I_0 \frac{eR_H}{k_B}(\xi/W_{\text{eff}})$, and where W_{eff} is the effective width over which the Hall voltage drops.

In the h-BN encapsulated graphene devices (S1 and S2 from objective 1), current curves could be superposed to temperature curves using a modified effective width that decreased linearly with an increasing current

$$W_{\text{eff}} = W_{I=0}(1 - \alpha \times |I|)$$

where $W_{I=0}$, the effective width at zero current, is found close to the sample width in S1 (5 µm) and at a lower value (less than 1 µm) in S2.

The current effect was also investigated by measuring the breakdown current I_c (defined by $R_{xx} > 0.1\ \Omega$). Similar breakdown current densities of approx 4 A/m were found in both S1 and S2 devices. The advantage of a larger T_0 in device S2 seems to be compensated by a lower$W_{I=0}$. Additionally, an inverse evolution of I_c is observed as a function of the gate voltage depending on the breakdown current polarity. These features can be explained by the relative effect of the Hall voltage to the graphite gate voltage. Given the small distance (approx 30 nm) of the graphite gate from the graphene layer, the applied gate voltages are significantly small and comparable to the Hall voltages that develop for the larger currents of a few µA used for metrology measurements. This suggests that the current circulation induces a differential gate effect on each edge of the Hall bar: V_g on one edge and $V_g \pm R_H \times I$ on the other edge. Which in turn, leads to a transverse carrier density gradient which then produces a transverse Landau level filling factor gradient in the QHE regime. The overall conclusions from the work were that the electronic transport properties can be strongly affected in devices equipped with a close gate by the current-induced gate shift effect, therefore this must be considered for metrological applications.

Small current detection in the QHE breakdown regime – The principle of small current detection uses the strong non-linear increase of the longitudinal resistance at the QHE breakdown to detect a small current variation. In the S1 and S2 devices (Objective 1) investigated, it was observed that the dynamic resistance increased with the DC current but remained limited to a few thousands of Ω. This small dynamic resistance could be explained by the determined dissipation mechanism which is dominated by the VRH.

Consequences for metrology – Detection of single Levitons in graphene by QHE breakdown is not yet possible. However, the above results have yielded important insights for the project and for the application of high mobility h-BN graphene and more generally van der Waals heterostructures in resistance metrology i.e.:

I. LNE observed the highest the carrier mobility and the highest temperature robustness of a quantum resistance standard,

II. the results on gating effects can be considered in the design of future graphene-based quantum resistance standards made from electric field-effect devices and

III. the studies of h-BN graphene heterostructures were a first step towards implementing van der Waals graphene heterostructures for Quantum Hall resistance standard application at a low magnetic field.

The above results are relevant for the implementation of devices equipped with a gate involving the quantum anomalous Hall effect at zero field.

4.2.2 A counting scheme for single-electron wave packets

Coincidence counting and single photon detection are crucial for assessing first and second order coherences in correlation measurements (Figure 8). The development of these techniques has been advanced by previous work in this field by their application in optical quantum information. By implementing networks of multiple detectors, multiplexing techniques or detectors with photon-number resolution, higher-order correlations have also become accessible. In an electronic analogue to optical interferometry experiments, the characterisation of single-electron and two-electron states as for example generated by tunable barrier electron pumps follows the same concepts for signal-acquisition.

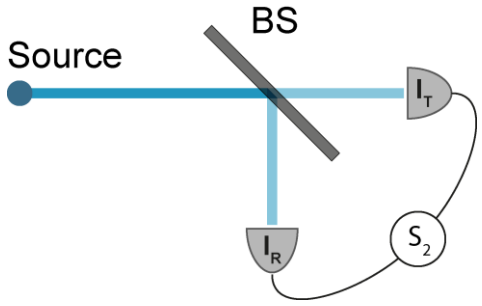

Figure 8 Schematic of a classic Hanbury Brown and Twiss experiment, where a time-correlated signal of the partitioning can be acquired using single-particle detection

While an electron source typically emits a highly regular stream and therefore does not induce a chaotic limit to correlation due to accidental coincidence, higher-order moments may still provide valuable information in the case of two-electron states and interactions. Similarly, the performance-criteria in the single-photon case, a detection and counting scheme for electron quantum optics should achieve high detection-efficiency, large bandwidth and the ability to resolve particle numbers with high fidelity. The following experimental results were gained at PTB.

In an electron quantum optics circuit as shown in Figure 3 (Objective 1), hot electrons injected in high magnetic field at non-equilibrium energies (several 10 meV above the Fermi level) propagate with minimal energy loss along the edge of the conductor (white lines exemplifying the path through the circuit). The detection of such quasi-ballistic electrons at the output of the circuit requires either storage [7] or on-the-fly readout techniques. Trapping electrons prior to readout allows significantly enhanced signal-to-noise at the expense of reduced bandwidth. Hot electrons can be trapped by controlled energy relaxation into a large charging node isolated from the remainder of the circuit. An example of the minimum essential circuit components is shown in Figure 3. In the micrograph of a GaAs/AlGaAs heterostructure, the etched mesa (dark blue) forms the conductive region, separated by Au top-gates into three sections forming the pump (red), a short wave guide with an edge-depletion gate (orange) used to modify transverse confinement potential for minimal losses, and a trapping node (green). The shape and size of the trapping node were designed to maximise the path length for the traversing electron while still allowing the charge to be read out with single- electron resolution.

A measurement of the probability of an electron to traverse the node $\alpha = I_T/I_0$ as a function of the entrance G_{N1} and exit G_{N2} barrier height can be used to illustrate the relaxation effects contributing to the effective detection fidelity (see Figure 9). As the barrier heights are raised, the maximum energy to which the node can be filled is increased, effectively decreasing the excess energy of the injection electron relative to the node. This then allowed the investigation of the energy dependence of relaxation effects with a fixed injection energy $E_0 = E_F$ in a continuous-current measurement ($I_0 \approx 48$ pA).

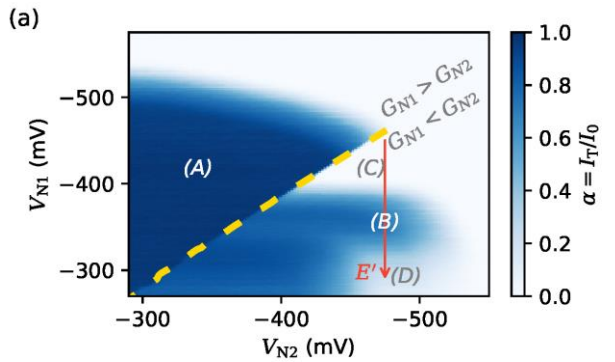

Figure 9 (a) Continuous-current measurement of the transfer coefficient $\alpha = I_T/I_0$ as a function of the node entrance and exit barrier-height for constant injection energy. Barrier heights increase to the top/right of the diagram. (b) Energy diagrams showing the path of scattered and transmitted electrons for various points labelled in (a): Electron relaxation can only be probed if not both scattered and transmitted electrons are collected in I_T (A); for an excess energy smaller than 36 meV LO phonon emission (D) is suppressed (B); below a threshold energy all incoming electrons are being scattered and not transmitted (C).

In Figure 9a, the dashed line denotes the symmetric barrier height ($G_{N1} = G_{N2}$). Below this dashed line, scattered electrons will flow over the lower entrance barrier and do not contribute towards the displayed exit-barrier transmission (see Figure 9b). The high injection energy isolates electrons from electron-electron (e-e) interactions within the wave-guide section of the circuit and transport along the gated edge suppresses relaxation via phonon emission (survival rate for this section of the path ≈ 0.998), however these effects become visible within the trapping node. At large and excessive energies (D in Figure 9a) Longitudinal optical (LO)-phonon emission is easily recognisable and requires the exit barrier to be at least 36 meV (the characteristic energy of LO-phonon emission in GaAs) below the injection energy in order for scattered electrons to still be transmitted.

With decreasing excess energy (below the 36 meV threshold) LO-phonon emission becomes suppressed and a large extent $\alpha \approx 0.6$ is observed, which is consistent with the fraction of electrons crossing G_{N2} without detectable energy loss when G_{N2} is formed.

For small excess energies e-e scattering dominates, displaying a power-law energy dependence down to a threshold energy, below which all electrons scatter before reaching the exit barrier (C in Figure 9). In addition to these two effects commonly observed in such circuits, back action from the charge readout will further increase the scattering rate within the trapping node. To trap an electron injected on-demand, excess electrons on the node are flushed by temporally lowering the entrance barrier, and the exit barrier is set to reflect all incoming electrons, forcing unscattered electrons on a roundtrip with a length of 10 µm. A trapping fidelity near unity (0.999) under a variety of experimental conditions was achieved by PTB making the trapping node a very robust and versatile building block for electron quantum optics.

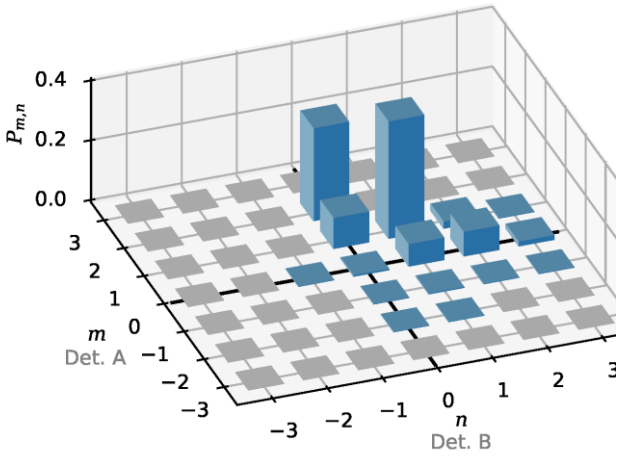

Figure 10 Exemplary bar graph depicting the coincidence correlations of two detector circuits (A and B), shown for a series of single-shot counting measurements. A total of 49 probabilities $P_{m,n}$ can be resolved by the electron counter.

For charge readout, the trapping node was capacitively coupled to a separate quantum dot which was tuned to a steep Coulomb blockade peak resonance, similar to conventional electron counting experiments. As the on-demand source provides control over the injection time, a differential readout of the charge detector signal with a high signal-to-noise ratio becomes possible, especially as the integration time of

the detector signal before and after electron injection can be freely chosen. At a readout bandwidth of 230 Hz, the exact number of trapped electrons was determined with a fidelity of better than 5σ.

For applications in tomography and interferometry, the required energy and time selectivity can be achieved by applying a sharp transient signal to the entrance barrier [7]. Figure 10 shows an example measurement of coincidence correlations $P_{m,n}$ in a configuration very similar to Figure 8, where the partitioning of a multi- electron state is acquired by placing two detection nodes (A and B) at the outputs of the beam splitter. With this a total of 16 different non-zero elements of the coincidence correlations were resolved. This also allowed the simultaneous characterisation of the source, which is important as this potentially injects unwanted extra electrons, records losses and excitations and probe interactions. This is particularly important in a system, where strong Coulomb interactions are likely to influence partitioning at the beam splitter as well as particle statistics. This work significantly exceeds the capabilities of current and noise measurements and highlights the project's important advantages in counting in complex circuits using multi-electron states.

4.2.3 Probing wave-packets emitted from on-demand single-electron sources

High energy quantum dot sources load and eject electrons from a dynamically formed quantum dot controlled by an RF drive waveform. Electrons within the two-dimensional electron gas (2DEG) from the trap region underneath the metal surface gates are released into high energy edge states, confined to the edge of the mesa by perpendicular magnetic confinement, as shown in Figure 11. There are several techniques which can be used to identify the characteristics of the excitations injected by this kind of source. A parameter-invariant quantised pump current $I_p = nef$ indicates that exactly *n* electrons are ejected within each cycle. Measuring the pump current for different pump drive waveforms (e.g. short versus long 'ejection' segments) can also give indirect information about the electron emission timing. However, to directly probe the emission distribution a time dependent barrier needs to be introduced in the beam path at distance from the pump, as shown in Figure 11. In such a device the electron injection energy *E* is measured by finding the (time-independent) detector gate voltage (V_{G3}) at which edge state current is transmitted as $I_T \simeq 0$. This is typically $E \simeq 100$ meV with a broadening of $\simeq 1$ meV. The barrier can also be controlled in a time-dependent manner by a signal generator phase-locked to the electron pump drive signal but with a relative delay t_{pd}. The 'detector' voltage can be modulated rapidly, alternating between voltages that open and close the channel to electrons at the injection energy. Transmission depends on the relative arrival time of the electron and the time when the barrier crosses the injection energy E. The proportion of electrons transmitted as a function of t_{pd} can be used to examine the arrival time distribution of electrons with picosecond resolution. This reveals that the arrival time distribution of single- electrons is typically < 10 ps in size and confirms that the emission process is very fast compared to the pump cycle time. It also demonstrates that the transport of electrons between the pump and detector (distance 2- 10 microns) does not introduce a gross broadening of the energy or arrival time distributions.

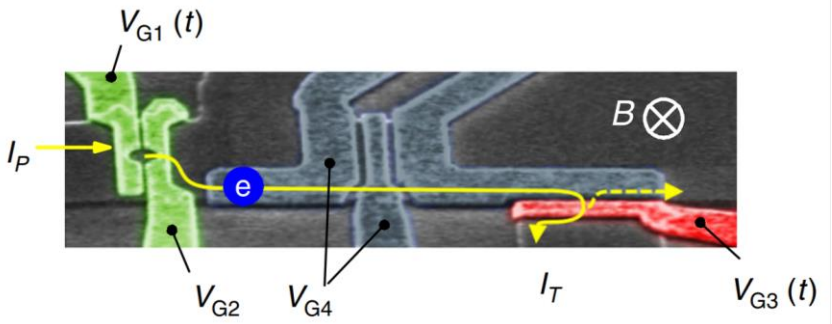

Figure 11: SEM micrograph of a tunable barrier pump (left, green) and time domain detector (red).

Although they have high resolution (~meV, ~ps), the above methods failed to capture several key details. For example, a significant modulation of the source dot voltage was expected during emission and led to a strong emission energy-time correlation, however the energy and time distributions alone did not capture this. In addition, information on the coherence of the single-electron excitations via tomographic reconstruction, as applied to the mesoscopic capacitor sources (see Objective 4, Section 4.4.1), is also highly desirable. But there was a serious problem when applying the same techniques to the higher energy injection, due to the

lack of a Fermi sea at the high injection energies of these sources. This means that another time dependent probe of the injected excitations is needed.

Therefore, the project decided to use the full temporal control of the detector barrier as a probe of the electronic Wigner distribution [4,6]. This method provided information about the energy time correlations by probing 'intermediate' projections of the distribution between the purely energy projection of a 'static barrier' measurement $I_T(V_{G3})$ and the (ideally) time-only projection of the rapidly opening/closing barrier $I_T(t_{pd})$. This is schematically shown in Figure 12a. A linear ramp of the barrier voltage creates a time dependent mask of the arrival time distribution, with only those parts in the 'open' ($T = 1$) side of the line of this filter contributing to the transmitted current. When the linear ramp rate of the detector is kept constant, but the DC offset voltage and/or time delay of the signal generator is swept, the current is cut off in a way that captures a particular projection of the distribution. Recording a large number of these projections (Figure 12b) and performing a numerical back projection (e.g. using the inverse radon transform) enabled computation of the arrival time distribution, as shown in Figure 12c.

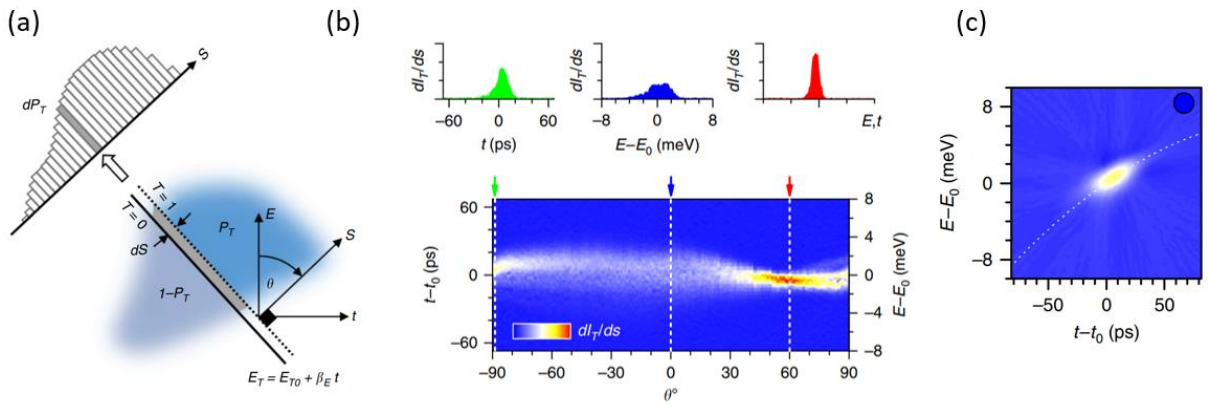

Figure 12: (a) Schematic of a partially transmitted emission distribution in the presence of a linear ramp of an energy filtering barrier (b) Example of data collected at a continuously varying range of cut angles in the energy time plane (c) Example of the numerical back-projection of data to form a map of the emission distribution.

The shape of the numerical back projections captured a pronounced correlation between the emission energy and time, with later arrival times corresponding to higher energy. This energy 'chirp' can be shaped by changing the sweep rate of the pump drive waveform near to the moment of electron emission. This experimental signature helped to establish that it was indeed the emission processes that imprints the correlation and not some other process relating to the propagation path or the detector. It also enabled a shaping of the distribution between maximal energy broadening (for fast emission) and maximal time broadening emission (for the slowest emission) which assisted the separation of contributions to the emission broadening.

The area occupied by the measured distribution in energy-time place is a relevant measure of the quantum mechanical purity of the injected wave packets when compared to the quantum limit of one Plank constant. The measured purity γ of the distributions indicates a distribution significantly broadened from that expected from quantum fluctuations alone with γ ~0.04. This suggests that some combination of experimental effects are broadening the detected emission distribution. One possible source is the effective energy resolution of the detector barrier, i.e. the energy range over which transmission changes from *T = 1* to *T = 0*. Changing the shape of the emission distribution allowed exploration of this factor. The smallest detected energy spread, was found to be $\sigma_{E,min}$ ~ 0.8 meV in the case of ejection from an almost stationary quantum dot energy, and represents an upper limit of the barrier resolution. The finite sweep rate of the experimental probe barrier was also a possible limiting factor on the temporal resolution. The experimental time broadening could be estimated from experimental parameters as σ_t ~ 0.3 ps. The estimates of the combined resolution, $\sigma_{E,min}\,\sigma_t$ ~ 0.36 $\hbar$, are smaller than the resolution required to resolve electronic emission broadened only by quantum uncertainty. Another possible source of the low experimentally detected purity was classical fluctuations of the quantum dot source, both in energy and in time; as any instability in the relative emission time will reduce the detected purity. In addition, effects relating to exact trajectories or loss in the beam path could also contribute. These classical effects should manifest themselves differently in different forms of interferometry, e.g. the interference

of single-particle amplitudes are expected to be less affected by emission time jitter, whereas two particle interferometry (e.g. in HOM geometry) require precise control of the arrival time of individual electrons in the same cycle.

Tomography techniques are a critical tool for benchmarking and optimising electron emission. The use of current measurements and dynamic barrier to perform tomography are a promising alternative path for accessing coherence information (see Objective 4, Section 4.4.2). This approach also has many interesting differences from the forms of tomography inspired by quantum optics, which rely upon an energy-selective barrier and would be antagonistic to two-particle interference. The complete absence of the Fermi sea in the conducting waveguide and scattering region also mean that the `solitary' electrons are in a different regime of environmental interactions, thus it is inevitable that novel tools are required to study excitations in this regime.

Even at a relatively low level of purity, the sharpness of the electron arrival time distributions is useful for characterising whichever waveform opens and closes the detector barrier and allows the full reconstruction of the gate waveform. This result represents a new and novel use for single-electron technology in the characterisation of RF signals at cryogenic temperatures.

4.2.4 Conclusions

Objective 2; to develop the metrological tools for the verification of single-electron sources required for the assessment and optimisation of the emitted electron wave packet states, including the characterisation of the dynamic electron state within the source quantum dot and the indistinguishability test of the travelling single-electron wave packet has been finished. There only remains model based analysis tools for the data gained in the indistinguishability experiments with high energy electrons, to be completed and this work is currently being finalised.

The characteristics of the QHE breakdown were studied by the project, on graphene grown by CVD on SiC and h- BN encapsulated graphene. This was done through the measurement of the temperature and current dependence of the dissipation. The project demonstrated the effect of a graphite gate close to the graphene layer on the QHE breakdown properties. The signal-to-noise still needs to be increased for single Leviton detection, nonetheless the project's results on the QHE breakdown mechanism are significant and highly relevance for the application of graphene in resistance metrology.

The project has successfully developed a tomographic measurement technique for the energy-time distributions for both high-energy (~ 100 meV) and low-energy (< 1 meV) electrons. The project's new tomographic measurement technique was used (i) to measure the dependence of the distribution of ejection conditions and (ii) to establish a connection between the dynamic change of energy in the emitting quantum dot to the phase space distribution of the electron. A model for single-electron emission from dynamic quantum dots was also successfully validated.

The project's tomographic measurement technique has also been used to set up ejection conditions for the two high-energy single-electron wave-packet sources used in a HOM geometry. The project investigated two-electron interactions in the HOM geometry for high-energy electrons. The results of the investigation showed that the behaviour in the high energy HOM systems is different to the low energy ones, due to the difference in screening of the coulomb interaction. This subject is addressed by the theoretical work on the collision of two interacting electrons on a mesoscopic beam splitter described in Objective 4 and Section 0.

The project has also examined the initial state preparation in the source dynamic quantum dot used for high energy electron preparation. To do this the project developed a model which was then validated by experimental data. The role of relaxation for the outcome of initialisation was also clarified by the project [2].

The project's newly developed tomographic techniques were also used to characterise the state, including the energy and time distribution, of electron wave-packets excited at low energy. In addition to high-energy and low-energy electron wave packets, a third type of electron wave packets were also examined in the project, these were excited by Lorentzian voltage pulses. The temporal width of this third type of electron wave packets was characterised, and for all three wave-packet sufficiently small temporal widths (< 1 ns) were observed [3].

4.3 Experimental techniques for on-demand single-electron wave packet interferometry for the sensing of local magnetic and electric fields with high time resolution (Objective 3)

Objective 3 for the project was to develop an experimental technique for on-demand single-electron wave packet interferometry for the sensing of local magnetic and electric fields with high time resolution (~ 1 ns or below) and high spatial resolution (~ 1 µm).

4.3.1 Single-electron interferometers for sensing

The principle of sensing by single-electron interferometry is shown in Figure 13a. A first beam-splitter splits electronic trajectories in two different paths that are recombined by a second beam-splitter. Inserting a time- dependent electric field on one arm of the interferometer leads to a temporal modulation of the phase difference between the two arms. Depending on this phase difference, electrons will exit the interferometer in output 3 or 4, which can be detected by either measuring the average electrical current or by detecting individual electrons using a single-electron detector. The time sampling of the electric field inside the interferometer can be performed by generating single-electron pulses of short temporal width at the input of the interferometer and recording the output interference pattern as a function of the time delay between single-electron emission and the time-dependent electric field.

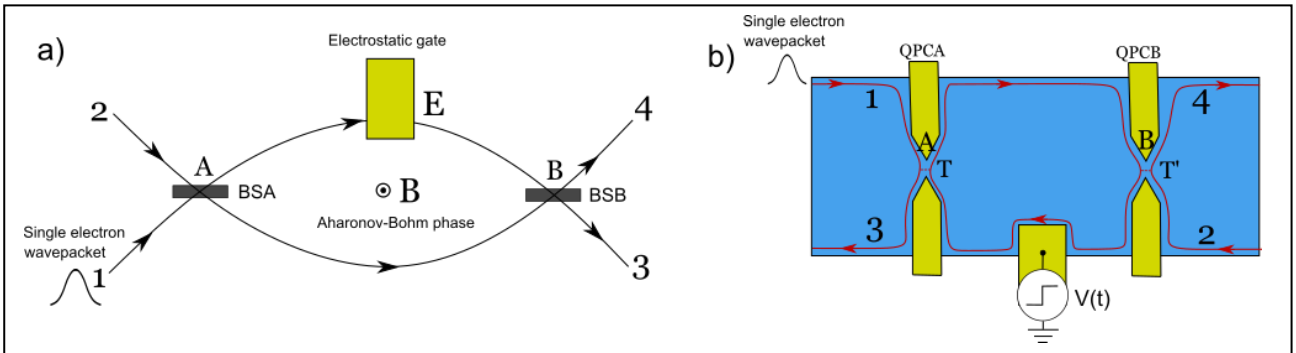

Figure 13 a) Principle of time-dependent interferometric sensing. Two beam-splitter define two paths for electron propagation. The electrical current at a given output of the interferometer probes the phase difference between the two paths which can be dynamically varied when a time-dependent electric field is generated at one arm of the splitter. using a single-electron source of short temporal width, the time dependent electric field can be sampled by measuring the output electrical current for different times of emission of electrons inside the cavity. b) Implementation of the previously discussed sketch in a Fabry-Perot cavity defined in a 2DEG in the integer quantum Hall regime. Electronic propagation occurs along the ballistic chiral edge channels (represented in red). Metallic split gates can be used as quantum point contacts used as electronic beam-splitters of tunable transmission amplitude t_A and t_B. Applying the time dependent voltage $V(t)$ on a plunger gate can generate a time-dependent phase difference between the two interfering paths.

Of the interferometer device types fabricated (see Objective 1, Section 4.1.6) the devices based on high-energy single-electron wave-packets did not show interference contrast. This could be attributed to insufficient purity of the emitted states as shown in the tomography experiments in Objective 2, Section 4.2.3. This led to averaging out the interferometric contrast in these devices. However, the developed tools were also used in follow up research to optimise the sources.

The following subsection describe the devices designed for low-energy single-particle wave-packets, work mainly performed by CNRS and CEA but with input from all other partners i.e. PTB, NPL, LatU. The subsections describe the realisation of these interferometers and their characterisation of the visibility for stochastic low-energy single-particles injected by a small applied voltage.

Fabry-Perot interferometer for low-energy single-electrons in GaAs/AlGas technology

In the presence of a strong magnetic field perpendicular to the sample (integer QHE regime), the electronic propagation can be guided along the edges of the sample, defining two distinct paths inside the interferometer with well-defined lengths. Figure 13b shows the design of an electronic Fabry-Perot interferometer in the integer QHE regime. Two split gates called quantum point contacts (QPCA and QPCB) act as tuneable beam-

splitters scattering electronic waves with transmission amplitude $t_{A/B}$ and reflection amplitude $ir_{A/B}$, where $t_{A/B}$ and $r_{A/B}$ are real coefficients. For $r_A, r_B \neq 0$, electrons can perform several roundtrips within the cavity of the Fabry-Perot interferometer, accumulating phase φ related to the Aharonov-Bohm phase inside the cavity. This phase can then be modulated by the voltage applied on the gate of the bottom part of the cavity (see Figure 13b). The time dependent electric field leads to a dynamical change of the area of the interferometer leading to a dynamical change of the Aharonov-Bohm phase.

The goal of this the work was to demonstrate sensing of electric and magnetic fields using single-electron wave packets with a time resolution below 1 ns and a space resolution of the order of 1 micron. The time resolution is limited by the width of electronic wave-packet whereas the spatial resolution is set by the size of the gate that is used generate the electric field.

A SEM image of the device used by CNRS for the following measurements is shown in Objective 1, Section 4.1.6 Figure 7e. It consists of a Fabry-Perot cavity, as shown in Figure 13b, implemented in a 2DEG of density n = $1.1 \cdot 10^{11}$ cm^{-2} and mobility μ = $1.4 \cdot 10^{6}$ $cm^2V^{-1}s^{-1}$.

A magnetic field B = 1.37 T was applied perpendicular to the sample in order to reach the integer QHE at filling factor $\nu = 3$ where the current is carried by three edge channels. In Objective 1, Figure 7e, two quantum point contacts labelled QPC1 and QPC3 were tuned to partially transmit the outer edge channel with transmissions T_A and T_B and fully reflect the two inner channels. QPC2 at the centre of the sample was used as a plunger, both for tuning the static value of the phase using a DC gate voltage and for applying the time dependent potential.

Figure 14 shows the measurement of the transmission through the cavity as a function of the DC gate voltage V_{dc} applied to the plunger and magnetic field B.

As can be seen in Figure 14, single- electron interferences were seen as oscillations of the transmission as a function of V_{dc}. The single-electron transmission amplitude of the oscillations was 0.18 and the contrast of interference was approx. 0.4.

The interference pattern appears unmodified when the magnetic field is varied. This is as expected when charging effects of the bulk of the interferometer lead to a shrinking of the interferometer area when the magnetic field is increased. However, oscillations of the transmission as a function of magnetic field were observed with an amplitude reduced by a factor 7 and a period of 0.6 mT which is consistent with a variation of the magnetic flux through the cavity of one flux quantum.

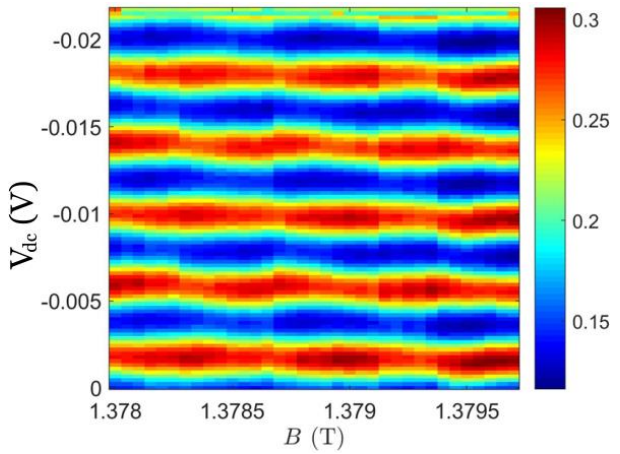

Figure 14: Two-dimensional colour plot of the transmission through the cavity as a function of gate voltage and magnetic field.

Graphene p-n junction Mach Zehnder interferometer

Graphene has several extraordinary properties, and these were used by CEA in a special band structure to develop an interferometer of extremely small area. The properties used were:

(i) single-layer graphene exhibits perfect electron-hole symmetry and zero gap at the Dirac point, which allows the smooth tuning of the density between the n and p regime in an appropriate heterostructure using a nearby gate.

(ii) In a magnetic field edge, state electron and hole edge states form in the n and p side respectively along the p-n junction and Klein-tunnelling is suppressed.

(iii) At a sufficiently sharp corner, controlled by additional gates, tunnelling between electron and hole edge states of opposite valley quantum number can be induced. This tunnelling was used to develop a gate controlled quantum-Hall p-n valley beam splitter; where the undisturbed edge states along the p-n junction form the wave guides within the interferometer, see Objective 1, Figure 7d.

Figure 15 shows the very good interference contrast achieved by CEA in the interferometer. From the magnetic field periodicity the area of the Mach Zehnder interferometer was determined to 0.15 μm^2, yielding a distance of 110 nm for the opposing edge states forming the interferometer [9].

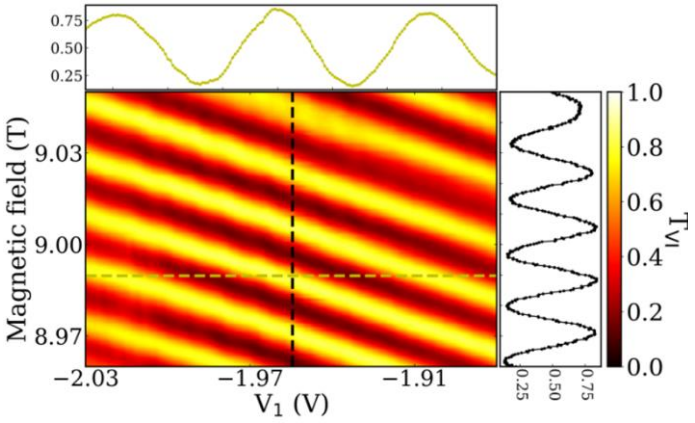

Figure 15: Interference pattern of graphene quantum Hall valley spitter based Mach Zehnder interferometer as function of side gate voltage and magnetic field.

4.3.2 Interferometric sensing of magnons in a graphene quantum Hall ferromagnet

When a perpendicular magnetic field is applied to a two-dimensional electron system (e.g. graphene), electrons become distributed in energy on widely-spaced, highly degenerate Landau levels, which are the hallmark of the so-called QHE regime. At large enough magnetic fields, the various symmetries underlying the Landau levels (spin, valley, etc) can break, giving rise to well-separated sub-Landau levels that can be fully polarised in a given symmetry. By tuning the electron density and the magnetic field such that only one spin- polarised sub-Landau level is filled, it is possible to create a perfect ferromagnet, i.e. a system where absolutely all electron spins point in the same direction. In monolayer graphene, such a perfect "quantum Hall ferromagnet" can be obtained at filling factor $\nu = 1$, when spin and valley symmetries are broken by electronic interactions and only a single spin- and valley-polarised electron channel can propagate along the edges of the sample (while the bulk remains insulated). Recent experiments outside of this project, have shown that it is possible to excite the elementary bulk excitations of this peculiar ferromagnet, (which are charge-neutral spin waves, or magnons), by applying to the sample a drain-source potential larger than the Zeeman energy. Many fundamental properties of these magnons still need to be observed and investigated. In particular, even though they are magnetic excitations, magnons of a quantum Hall ferromagnet have an intrinsic excitonic nature, as they carry an intrinsic electric dipole oriented perpendicularly to their propagation direction.

To investigate this electric dipole, CEA devised an experiment [14], shown in Figure 16a, in which a stream of magnons is emitted towards an electronic Mach-Zehnder interferometer realised in a graphene p-n junction as described in Section 4.3.1, which acts as an ultra-sensitive electric dipole detector. The CEA detection mechanism was two-fold:

I. the stream of magnons impinge on the interferometer with a given average angle, which depends on the position of the magnon emission point relative to the interferometer. Depending on the value of this angle, the positive part of the electric dipole might be closer to the interferometer than the negative part, or vice-versa (see Figure 16a). This plays the role of an effective local electrostatic gate, shifting the position of the interferometer's two arms (central blue and yellow arrows shown in Figure 8) relative to one another, thus leading to a measurable phase shift of the interferometer.

II. the magnons are emitted randomly in time and impinge accordingly on the interferometer. This leads to rapid fluctuations in the electric field felt by the interferometer, which cause the amplitude of the interference pattern to diminish.

CEA confirmed the above dual effects in their experiments (see Figure 16b) and demonstrated the first ever observation of the excitonic nature of magnons in a quantum Hall ferromagnet.

Furthermore, the analysis of the results unveiled several elusive properties of the magnons; amongst them, the fact that the emission process is Poissonian (that is, magnons are indeed emitted randomly in time), and that increasing the drain- source potential increases the magnons' emission rate rather than their energy [14]. These results demonstrate for the first time the ability to couple magnetic excitations to quantum coherent

conductors and highlight many exciting possibilities for experiments probing new phenomena at the intersection of mesoscopic quantum physics and spintronics.

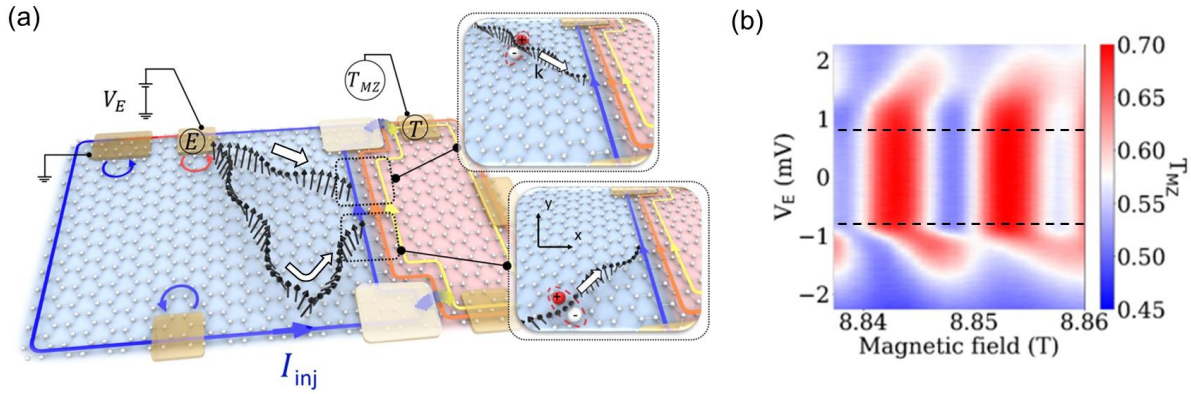

Figure 16 (a) Artist sketch of the experiment: a flake of graphene is divided into two regions with opposite p- and n-doping (blue and red areas), creating at their interface an electronic Mach-Zehnder between the edge channels of each region with same spin (blue and yellow arrows). An additional channel with opposite spin (red arrow) also propagates in the right region but does not play any role here. Magnons (wavy black arrows) are emitted from a biased contact (E) towards the interferometer. Depending on the propagation direction relative to the interface (symbolized by the large white arrows), the magnons' electric dipoles (red and white balls) can have different orientations when impinging on the interface, as depicted in the insets. (b) Electronic transmission TMZ across the interferometer, measured versus bias voltage V$_E$ and magnetic field. Above the bias voltage threshold (black dashed lines), magnons are emitted and the interference patterns become tilted and significantly blurred, indicating phase shift and decoherence.

4.3.3 Time dependent field sensing by single-electron interferometry

Having characterised single-electron interferences through the Fabry-Perot cavity for stochastic single-electrons in Section 4.3.1, the project moved on to the demonstration of time resolved interferometric sensing of a time dependent field. To do this CNRS applied a periodic square voltage V(t) at a frequency of 1 GHz on the top split gate of QPC2 (see Objective 1, Figure 7e) which led to a dynamic variation of the phase of the electrons traversing along this side of the Fabry-Perot cavity and the measurement of the transmission coefficient of a single-electron wave packet of Leviton type with 35 ps width through the Fabry-Perot cavity. The single-particle nature and the shape of the wave packet were characterised beforehand by quantum state tomography.

Figure 17 shows the measurement of the transmission through the Fabry-Perot cavity as a function of the DC voltage (V_{dc}, vertical axis) and the time delay (horizontal axis) between the single-electron emission and the periodic square voltage applied to the top split gate.

Taking a vertical cut of the colour plot shows the oscillation of the transmission as a function of the static phase difference for a given time delay. At a time delay of 300 ps, CNRS observed a sudden shift of the interference pattern (with a phase shift which equals π/2). This reflected the fact that single- electrons were now sensing a different value of the electric field (or electrical potential) corresponding to a modified value of the phase difference between the two paths inside the Fabry-Perot interferometer. The interference pattern then stayed roughly constant until, at a time delay of 800 ps, the interference pattern shifts again as the square voltage

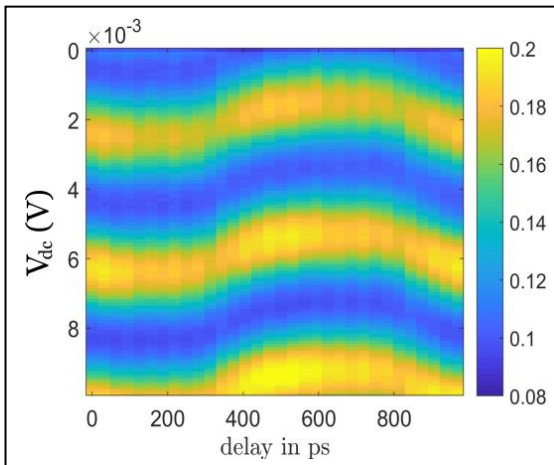

Figure 17: Transmission coefficient as function of single-electron wave packet delay and of DC control voltage with a 1 GHz square wave voltage applied to a gate on one side of the Fabry Perot interferometer.

goes back to its initial value. The plot in Figure 17 shows that single-electron pulses combined with single-electron interferometry can be combined to detect time- dependent electrical potentials with a time resolution of approx 100 ps and a spatial resolution < 1 μm corresponding to the width of the gate finger.

4.3.4 Conclusions

The project has developed and demonstrated time resolved sensing by interferometry of on-demand single-electron wave packets and has fulfilled the targets of Objective 3; to develop an experimental technique for on-demand single-electron wave packet interferometry for the sensing of local magnetic and electric fields with high time resolution (~ 1 ns or below) and high spatial resolution (~ 1 μm).

The transmission of single electrons through a Fabry-Perot cavity was studied for single-electron wave packet interferometry. The project observed a modulation of the transmission of single-electrons with a contrast close to 20 % when varying the magnetic field and more than 50 % when varying the gate voltage at a plunger gate at one side of the cavity. The project also used the variation of the current with the plunger gate voltage in order to sample the time-dependent electric field generated by a time dependent voltage locally at plunger gate. By varying the delay between the emission of single electron pulses and the time-dependent voltage, the local potential of the Fabry-Perot cavity was sampled as a function of time. The sampling time resolution was approx 0.1 ns (close to the limit imposed by the width of single electron pulses) and the space resolution was < 1 μm corresponding to the width of the gate finger. The project also found that time dependent magnetic field sensing is possible analogous with a spatial resolution corresponding to the typical size of the cavity (2 μm for the smallest cavity).

A Mach-Zehnder type interferometer of much smaller size was developed based on the quantum Hall valley beam splitter (developed in Objective 1) in a p-n-junction in graphene with an active area of 0.15 μm^2. A strong current modulation with visibility of nearly 1 as function of applied magnetic field and side gate voltage was demonstrated by the project and can be used as the basis for future wave-packet, time dependent sensing of magnetic fields with sub-micron resolution.

Further to this, the project demonstrated graphene based interferometric sensing: the interferometric signal in the p-n-junction device was very sensitive to a phase shift and to decoherence due to excitations generated in the quantum Hall system, whose edges are used to form the wave guides of the interferometer. For a quantum Hall ferromagnet, at a filling factor $\nu = 1$ with full valley and spin polarisation of the electrons, the low energy excitations carry a magnetic moment and are called magnons. The effect of these magnons on the single-particle wave packets traversing the p-n junction interferometer was successfully demonstrated by the project and used to extract information on the magnon emission process.

4.4 Concepts and theoretical tools for full quantum state tomography and quantum enhanced sensing (Objective 4)

Objective 4 for the project was to develop concepts and theoretical tools for full quantum state tomography to enable the realisation of quantum enhanced measurements using electron wave packets. Within this objective, methods for quantum state tomography were developed and demonstrated. For low-energy electrons a HOM-type collision setup (see Objective 1, Section 4.1.5) can be used: the unknown single- electron wave-packet interferes at a beam splitter with a known reference signal and is then analysed. However, this method is not directly applicable for high energy electrons and thus a different approach was developed by the project, that uses a dynamic barrier.

4.4.1 Quantum state tomography of low-energy single-electron wave packet states

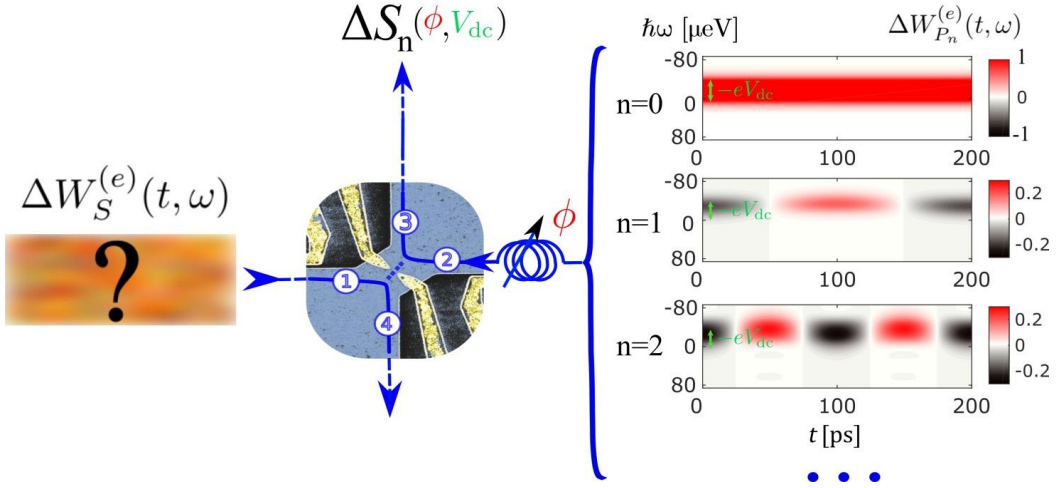

Figure 18: Quantum current analyser for low energy excitations. Interference between the unknown periodic electronic Wigner distribution $W_S^{(e)}$ in the incoming channel (1) and a modulated reference Fermi sea signal $W_{P_n}^{(e)}$ incoming in channel (2), generated by a voltage $V_{P_n}(t)$ applied to a contact, occurs at a central barrier. The current and shot noise signals in the outputs (3) and (4) are readout (noise readout techniques as per section 4.1.2). The measurement is repeated with a set of known reference signals at harmonics of the base frequency of the unknown signal.

A method for reconstructing the Wigner function of electronic states injected at low energies was developed and demonstrated by CNRS. The method uses the interaction between the injected excitations and a modulation of the Fermi sea level of a reservoir on the other side of a beam splitter. The injected electronic signal was then investigated with a variety of AC modulations phase locked to the source. Shot noise was used as readout of the correlations in the electronic scattering at the central barrier.

A numerical process of deconvolution was used to extract the relevant signal and to compute the energy time distribution. This numerical process constituted a 'quantum current analyser' (see Figure 18). The analysis result for a wave-packet generated by a Lorentzian voltage pulse is shown in Figure 19. The voltage pulse was chosen in order to generate a single-electron Leviton. The decomposition into the 1-electron and 2- electron contributions shows a dominating weight ($g_1^{(e)} = 0.82$) of a single-electron wave-function with $\tau = 42$ ps width. The finite value of purity agrees with expectation due to finite temperature of $T = 50$ mK [3].

The tomography protocol was further refined by the introduction of a signal-processing algorithm based on orthogonal elementary single-particle states, the electronic atoms of signals [11]. This was an important step for the project and represents as move towards a signal processing of quantum electrical currents that is applicable far beyond experiments with single-electron wave packets.

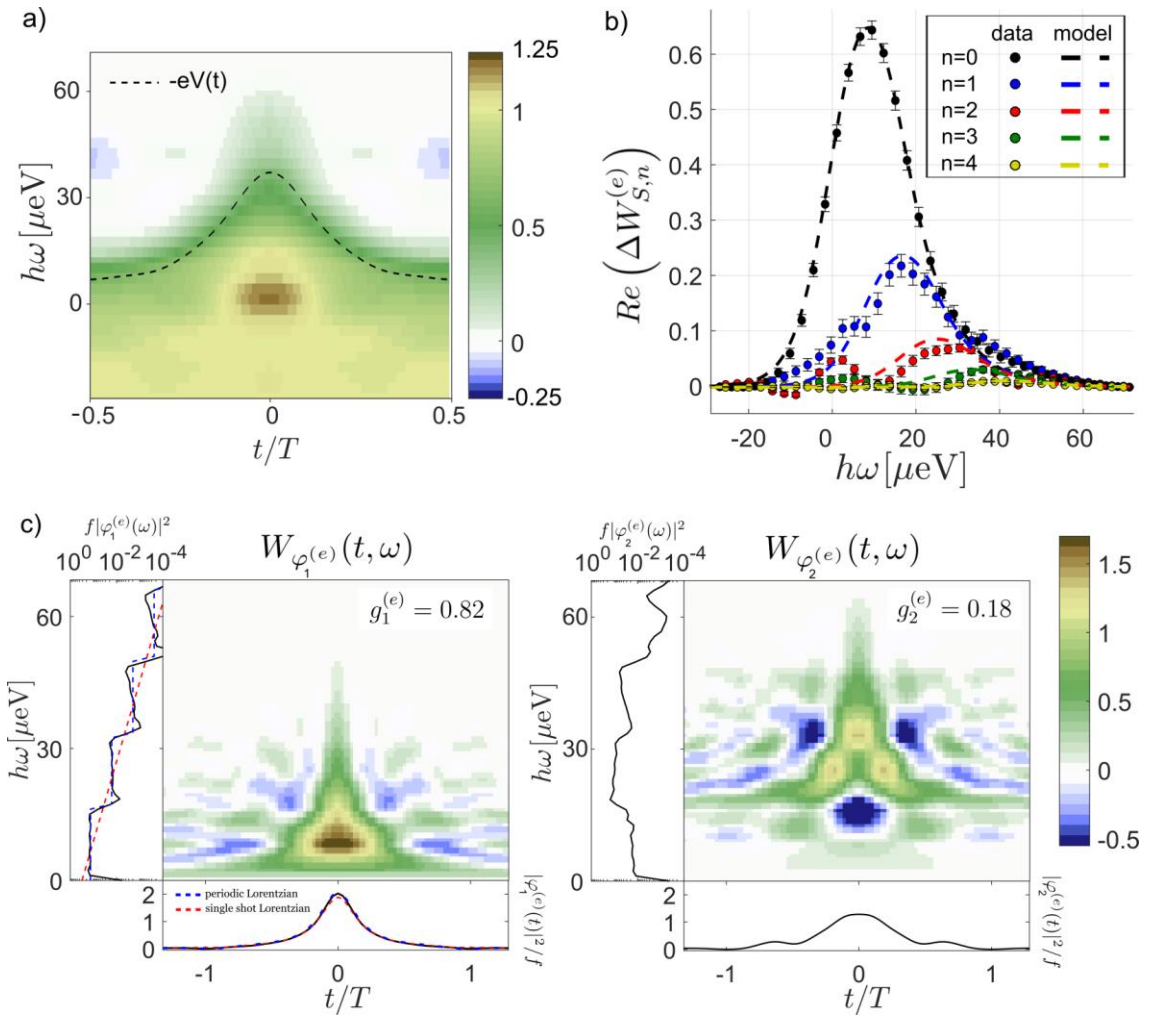

Figure 19: (a) Reconstructed electronic Wigner function generated by a Lorentzian voltage pulse. (b) Contributions at the different harmonics. (c)+(d) Decomposition into the 1-electron (c) and 2-electron (d) contributions to the Wigner function.

4.4.2 Quantum state tomography of high-energy single-electron wave packet states

A method for quantum state tomography of isolated high-energy electron wave-packets was developed [6] using an energetically sharp partitioning barrier that is also gated by time-dependent potential. Using the spatially uniform gating of the scattering region, the probability of single-shot transmission can be expressed in a compact analytic form in terms of the energy-dependent transmission function T(E) of a static barrier, the time-dependence of the modulation potential V(t), and the Wigner representation of incoming electron's wave-function. More generally the ensemble sampled by the source of electrons incoming one-by-one can be represented by the quantum mechanical single-particle density matrix which can represent a mixed state, and in the limit of low purity – a classical probability density in continuous phase space.

According to this theoretical result, an isolated wave-packet scattering on a modulated partition barrier with a subsequent high-fidelity readout constitutes a so-called positive operator-valued measure (POVM) that can be tuned by choosing an appropriate reference wave-form V(t).

In the limit of an energetically sharp barrier, the POVM became a projective measurement and all uncertainty in the scattering outcome came from the uncertainty in the incident wave packet. The latter also contained inevitable Heinsberg broadening as well as classical time jitter and potential incoherent energy broadening, encoded in a mixed-state Wigner density. The observables measured also depend on the choice of the time- dependent reference V(t) and are generally quantum-mechanically incompatible. This is a very important

fact and paves the way for the development of tailored tomography protocols conceptually similar to the HOM-interferometry-based tomography in Figure 18, but based on a different physical principle. Table 1 shows a comparison between these two complementary tomography frameworks.

	Low-energy electrons	High energy solitary electrons
Physical principle	Two-particle interference	Energy-selective transmission
Reference signals	Time-dependent bias creating controlled quantum excitations in a cold Fermi sea	Time-dependent gate voltage defining a controlled quantum variable realised by a sharp partitioning barrier
Beam splitter	Spectrally flat	Energy-selective
Measured signal	Cross-correlation noise	Transmission probability (current)
Quantity used for quantum state reconstruction	Quantum overlap between unknown and reference wave-functions	Projection of the wave-function onto a reference observable
Main purity-limiting factor	Electronic temperature	Energy selectivity of the barrier

Table 1 Qualitative comparison of the tomography protocols of low-energy and high-energy electronic excitations

This important theoretical result on the probability of scattering by a modulated barrier can be interpreted in several physically equivalent ways. A particularly useful case is that of a linear modulation where the projected observable is a linear combination of two canonically conjugate continuous variables (position/momentum or locally equivalently, arrival-time/energy). In this case of linear modulation, the spatial extent of the time-dependent electric field experienced by the wave-packet as it enters under the modulating gate is cancelled out. This then relaxes the conditions for applying the formula to a single-gate structure where both scattering, and time-dependent potential modulation are controlled by a single gate [4].

An additional advantage of the linear modulation is that the quantum scattering process permits a classical interpretation. In this classical interpretation of the exact total scattering probability formula the quantum Wigner function plays the role of quasi-probability density for the electron to arrive at a specific energy and a specific time and then scatter with a probability corresponding to the instantaneously barrier height, $T[E - eV(\mathrm{t})]$. The advantage of this classical interpretation is that it has a natural classical limit in which the Wigner density is positive and much less than one (in the quantum unit of phase space area, namely the Planck constant h). This semiclassical regime with a linearly modulated barrier was explored experimentally by partners NPL and LatU [4] in Objective 2, Section 4.2.3 and Figure 12.

The standard quantum limit for the characterisation of the electrical current at the level of first-order coherence [11] is a quantum-noise-limited measurement instantiated by ideal tomography protocols. A particular quantitative measure of distance to the quantum limit for both the low-energy and the high-energy protocols is a quantum mechanical purity which is defined as the trace of the quantum mechanically density matrix or equivalently as the average phase-space area per electron in the reconstructed Wigner distributions. For low-energy electrons a purity of order one was experimentally demonstrated by CNRS [3]. However, an approach for the quantum limit in high-energy electron tomography requires further work. This can be done using the tomographic tools developed in the project to benchmark and optimise the emission state purity and validate the dynamical time-dependent scattering formula in the non-linear regime [6].

Two-electron tomography is more challenging for high-energy electrons than for low-energy many-body excitations. The theory for low-energy many-body excitations benefits from efficient screening of electron-electron interactions. The single Fock-state approximation enables local reduction of the second order coherences to the first order ones in direct analogy to photonic HOM interference.

In contrast for isolated high-energy electrons the interactions may be under-screened and quantum interference effects due to wave-function overlap could be suppressed by Coulomb repulsion at short distances. LatU performed *ab initio* theoretical modelling of such Coulomb-interactions-dominated regime for two-electron partitioning by a sharp energy barrier [arXiv: 2201.13439]. This two-dimensional saddle-point

potential model with long-range Coulomb interactions was used to produce figures of merit for the strong-coupling (interaction-dominated) regime. The project expects that classical effects will dominate over HOM interference when the phase shift induced by one electron on the other electron significantly exceeds the full circle of 2π, or, equivalently, when the one electron wave-packet is shifted by the presence of the other electron in phase space over an area much larger that the quantum unit of Planck constant h.

In addition, to tomography protocols for isolated electrons, important future application of the dynamic partitioning formula [6] is a complementary to quantum-limited metrology of fast waveforms with pre-calibrated single-electrons wave packets. A principle of single-electron sampling oscilloscope has been proposed and demonstrated at the classical level prior to the start of this project [Johnson, N., et al, Appl. Phys. Lett. 110, 102105 (2017) https://doi.org/10.1063/1.4978388]. The project has built on this and found that characterisation of the collected signal as a quantum POVM can be used as the foundation for quantum metrology analysis of the sensitivity for such a sampling oscilloscope. The general theory of quantum signal carried by electrical currents [11] leads to a formal equivalence between dynamical scattering of one electron on a modulated barrier as well as the quantum mechanical overlap between the corresponding single-electron wave-function and an effective Fermi sea. This demonstrates the quantum limit on the single-shot readout of a fast transient voltage pulse: i.e. the minimal area under a voltage pulse that can be unambiguously detected by scattering of a single-electron is Planck constant h divided by the elementary charge e.

4.4.3 Conclusions

Quantum tomography protocols both for low-energy and for high-energy electrons have been studied and developed by the project. The targets of Objective 4; to develop concepts and theoretical tools for full quantum state tomography to enable the realisation of quantum enhanced measurements using electron wave packets. were fulfilled.

A protocol was developed for the quantum tomography of single-electron wave packets using dynamic scattering and was applied to the experimental data (from objective 2) for the measurement of the energy-time distribution of high-energy electrons. The protocol was also used to measure the quantumness of the wave-packets, as this is an important characteristic for interferometry.

Further to this, the developed protocol for the quantum tomography of single-electron wave packets was used (i) for the optimisation of the wave packet source for emission of states with higher purity and (ii) for the characterisation of the quantum state properties. The effect of experimental RF bandwidth on the fidelity of tomography results was also investigated.

The project theoretically studied quantum scattering of single-electron wave-packets by dynamical barriers and used the results to optimise the new tomography protocol. The results of the theoretical study were also used to establish a theoretical framework to determine quantum limits on resolution of single-electron signal-sampling techniques.

The project developed a method for the control of the overlap of split wave packets in the Mach-Zehnder geometry for high-energy electrons. It did this by tuning their drift velocity in the split paths independently. Decoherence effects in high-energy Mach-Zehnder interferometry were also studied and strategies for improving the visibility of interference were determined. In addition, analytical and numeric modelling of Mach- Zehnder interferometry with realistic energy-time distributions of high-energy single-electron wave packets were used to examine the effect of asymmetric arm length. The results of this revealed additional design criteria needed for optimising interferometer visibility.

A quantum tomography protocol for low-energy electrons was developed by the project. It was based on the experiments on the HOM geometry from objective 1. The quantum tomography protocol for low-energy electrons was used to characterise the temporal and energy distributions of low-energy single electron wave packets. The protocol also provides information of the purity of the emitted state and can thus be used to characterise precisely by how much they deviate from pure electron states. In particular, it establishes the crucial role of thermal fluctuations in reducing the purity of low- energy single electron states. The tomography protocol for low-energy electrons was further refined by the project, by the introduction of a signal-processing algorithm based on orthogonal elementary single-particle states, the electronic atoms of signals. This project output is an important step towards the signal processing of quantum electrical currents.

5 Impact

The project has fostered the application of single-electron wave packet devices for quantum metrology and the European metrology capabilities for quantum technology through (i) training workshops for partners, stakeholders and collaborators, (ii) publications, (iii) conference presentations, and (iv) liaisons with relevant industries and standards bodies. In particular contact with the Quantum Community Network, which is part of the Flagship on Quantum Technologies governance structure, was established and one of its members, become a member in our project's Stakeholder Committee.

Impact on industrial and other user communities

The early uptake of the project's results by industry has already occurred and is expected to continue. Examples include:

- Two stakeholder institutions (KRISS (the Korean NMI) and the Korea Advanced Institute of Science and Technology (KAIST) have started to implement single electron quantum optics experiments from Objectives 1 & 2 following discussions with the consortium.
- Partners PTB and NPL have had discussions with scientists at the basic research laboratory of stakeholder Nippon Telegraph and Telephone Corporation (NTT in Japan), on the implementation of single electron quantum optics techniques from Objectives 1 & 2 in silicon based single electron devices manufactured at NTT.
- Partner NPL engaged with an industrial supplier of RF components used to carry the microwave signals that control and readout qubits in prototype quantum computers. The project's new measurement capabilities on hot electron quantum optics in Objective 1 could be used to test and validate elements in the RF signal chain, particularly those at low temperature. Tests of cryogenic multi-terminal RF interconnects have been conducted with Intelliconnect, who are a leading manufacturer of RF connectors, adaptors and cable assemblies.

More generally, the uptake of the project's local time resolved sensing of electric and magnetic control fields (Objectives 2 & 3) into devices used for quantum technology development and evaluation, should allow the direct measurement of these fields at relevant time scales and support the development of scalable semiconductor technology for quantum computation and simulation. Similarly, the adoption of the project's quantum tomography techniques (Objective 4) is expected as a diagnostic tools to support the evaluate the performance of quantum state control and manipulation in dedicated technology test applications. Further to this, the project's demonstration of magnon detection (Objective 3) and examination by single-particle interferometry has shown the prospect of quantum sensing of a wider range of signals.

Impact on the metrology and scientific communities

The project has disseminated its outputs to the metrology and scientific communities via 14 open access publications in journals such as Physical Review X, Physical Review Letters, Nature Communications and Nature Physics, as well as 34 posters/presentations at conferences.

The project's results have advanced research in electron quantum optics and introduced new technologies like single-electron detection (Objective 1 & 2) and new concepts for quantum state tomography (Objective 4). The project has also advanced the understanding of the QHE breakdown in high-mobility encapsulated graphene (Objective 2). Furthermore, the project's new experimental tools for on-chip time resolved sensing and advanced single wave packet detection and characterisation (Objectives 2 & 3) will advance academic research on quantum physics in solid state systems.

The project's research on the optimisation of high-energy single-electron pumps (Objective 1 & 2) will also be used in further improvements of single-electron quantised current pumps for the realisation of the quantum ampere in the new SI [10]. The understanding of the electron back-tunnelling and emission processes examined in [2,4,7] is directly related with the accuracy of single-electron sourcing. A very recent result of the project published as preprint [arXiv: 2112.10713] on new schemes for operating high-energy single-electron sources could also allow easier operating conditions for single-electron pumping for quantum current generations. This work will be furthered in the electrical quantum metrology activities at partner PTB. A further improvement for quantised current sourcing is the use of fast time dependent beam-splitters as used in Objective 2 [4] for a filtering of erroneously sourced electrons. This work will be furthered in the electrical quantum metrology activities at partner NPL.

The project's liaisons with the quantum technology community have resulted in participation in a technology roadmap paper on quantum nanotechnologies, in which partners contributed a section on applications of high energy single-electron sources for metrology [10].

The project engaged with a stakeholder (University of Waterloo) from the quantum technology community who had special device fabrication knowledge. This collaboration resulted in the validation of dopant-free single-electron technology for use in quantum metrology [12] and offers a new path towards jitter-free single-electron wave-packet based quantum optics devices with improved performance.

The project's results on dissipation mechanisms in high mobility h-BN graphene in the QHE regime and the study of gating effects (Objectives 2) have provided a first step towards implementing van der Waals graphene heterostructures for quantum Hall resistance standard application at low magnetic fields. These results are also relevant for the implementation of devices equipped with a gate involving the quantum anomalous Hall effect at zero field. Follow on work is already planned at partner LNE.

To encourage uptake and dissemination to a wide range of stakeholders in the metrology and scientific communities the project held two internal workshops. The first was a workshop on single electron quantum optics for quantum enhanced measurements in October 2019, which gave an overview of the state-of-the-art metrology research, including results from the project. The second workshop on Quantum Electrical Metrology, was a foresighting exercise, and provided an opportunity to see how such emerging technology may meet long term societal challenges and end-users needs. Finally, a 2-day final online project workshop with more than 100 participants was organised by the consortium in October 2021. This workshop had participants from 14 countries, representing key stakeholders, the metrology community and the quantum science research community. The workshop was on Single-Electron Quantum Optics for Metrology and was preceded by introductory tutorials, followed by presentations from the consortium and renown researchers from the field of quantum technologies.

Impact on relevant standards

Due to the early stage of quantum technology, no standards currently exist yet for quantum information processing or for other electronic quantum bit-based devices. However, the commercialisation of such technology will require standardisation for relevant properties of quantum states or quantum devices and procedures for measurement or verification. This project has contributed important knowledge to standardisation bodies in the areas of electrical quantum metrology in order to foster the production of future standards. Project partners of the project have participated in and presented the results of the project to EURAMET Technical Committee Electricity and Magnetism (TC-EM) Sub-committee (SC) DC and Quantum Metrology, IEC TC 113 Nanotechnology for electrotechnical products and systems WG3 Performance assessment, DKE K 141 Nanotechnology and BIPM and CIPM's Consultative Committee for Electricity and Magnetism (CCEM).

Longer-term economic, social and environmental impacts

This project has developed new measurement techniques to support the development of semiconductor quantum technology in Europe. The project's new techniques were based on the use of on-demand single-electron quantum optics and have enabled the characterisation of (i) the quantum state of electrons in semiconductor quantum devices and (ii) quantum enhanced sensing based on the technique of single-electron quantum optics. The project's outputs have provided underpinning metrology for the rapidly evolving field of quantum technologies, thereby supporting future IT technology, the European IT industry, and hence future employment in this sector. In the longer-term, the research and development of scalable quantum solid state technology will be a key technology for future applications and high-tech products is highly beneficial for the advancement of the European information technology industry.

6 List of publications

1. C. Emary, L. A. Clark, M. Kataoka, and N. Johnson, *Energy relaxation in hot electron quantum optics via acoustic and optical phonon emission*, Phys. Rev. B **99**, 045306 (2019). DOI:10.1103/PhysRevB.99.045306

2. T. Wenz, J. Klochan, F. Hohls, T. Gerster, V. Kashcheyevs, H. W. Schumacher. *Quantum dot state initialization by control of tunneling rates*. Phys. Rev. B **99,** 201409(R) (2019). DOI:10.1103/physrevb.99.201409
3. R. Bisognin, A. Marguerite, B. Roussel, M. Kumar, C. Cabart, C. Chapdelaine, A. Mohammad-Djafari, J.-M. Berroir, E. Bocquillon, B. Plaçais, A. Cavanna, U. Gennser, Y. Jin, P. Degiovanni and G. Fève *Quantum tomography of electrical currents,* Nature Communications **10**, 3379 (2019). DOI:10.1038/s41467-019-11369-5
4. J. D. Fletcher, N. Johnson, E. Locane, P. See, J. P. Griffiths, I. Farrer, D. A. Ritchie, P. W. Brouwer, V. Kashcheyevs and M. Kataokam, *Continuous-variable tomography of solitary electrons,* Nature Communications ***10***, 5298 (2019). DOI:10.1038/s41467-019-13222-1
5. W. Poirier, S. Djordjevic, F. Schopfer, O. Thévenot, *The ampere and the electrical units in the quantum era*, C. R. Phys., 20, 92 (2019). DOI:10.1016/j.crhy.2019.02.003
6. E. Locane, P. W. Brouwer, V. Kashcheyevs, *Time-energy filtering of single electrons in ballistic waveguides*, New J. Phys. **21**, 093042 (2019). DOI:10.1088/1367-2630/ab3fbb
7. L. Freise, T. Gerster, D. Reifert, T. Weimann, K. Pierz, F. Hohls, N. Ubbelohde. *Trapping and Counting Ballistic Nonequilibrium Electrons.* Phys. Rev. Lett **124**, 127701 (2020). DOI:10.1103/PhysRevLett.124.127701
8. L. A. Clark, M. Kataoka, and C. Emary, *Mitigating decoherence in hot electron interferometry*, New J. Phys. **22**, 103031 (2020). DOI: 10.1088/1367-2630/abb9e5
9. M. Jo, P. Brasseur, A. Assouline, G. Fleury, H.-S. Sim, K. Watanabe, T. Taniguchi, W. Dumnernpanich, P. Roche, D. C. Glattli, N. Kumada, F. D. Parmentier, and P. Roulleau, *Quantum Hall Valley Splitters and a Tunable Mach-Zehnder Interferometer in Graphene.* Phys. Rev. Lett. **126**, 146803 (2021). DOI:10.1103/PhysRevLett.126.146803
10. A. Laucht, F. Hohls, N. Ubbelohde et. al., *Roadmap on quantum nanotechnologies*, Nanotechnology **32**, 162003 (2021). DOI:10.1088/1361-6528/abb333
11. B. Roussel, C. Cabart, G. Fève, and P. Degiovanni, *Processing Quantum Signals Carried by Electrical Currents*, PRX Quantum **2**, 020314 (2021). DOI:10.1103/PRXQuantum.2.020314
12. B. Buonacorsi, F. Sfigakis, A. Shetty, M. C. Tam, H. S. Kim, S. R. Harrigan, F. Hohls, M. E. Reimer, Z. R. Wasilewski, and J. Baugh, *Non-adiabatic single-electron pumps in a dopant-free GaAs/AlGaAs 2DEG*, Appl. Phys. Lett. **119**, 114001 (2021). DOI:10.1063/5.0062486
13. C. J. Barratt, S. Ryu, L. A. Clark, H.-S. Sim, M. Kataoka, and C. Emary, *Asymmetric arms maximize visibility in hot-electron interferometers*, Phys. Rev. B **104**, 035436 (2021). DOI:10.1103/PhysRevB.104.035436
14. A. Assouline, M. Jo, P. Brasseur, K. Watanabe, T. Taniguchi, Th. Jolicoeur, D. C. Glattli, N. Kumada, P. Roche, F. D. Parmentier and P. Roulleau, *Excitonic nature of magnons in a quantum Hall ferromagnet*, Nature Physics volume **17**, 1369–1374 (2021). DOI:10.1038/s41567-021-01411-z

This list is also available here: https://www.euramet.org/repository/research-publications-repository-link/

7 Contact details

Dr Frank Hohls, PTB

Tel: +49 531 5922530

E-mail: frank.hohls@ptb.de